Stellar neutron capture cross sections of the Lu isotopes

K. Wisshak, F. Voss, and F. Käppeler*

Forschungszentrum Karlsruhe, Institut für Kernphysik, Postfach 3640, D-76021 Karlsruhe, Germany

L. Kazakov

Institute for Physics and Power Engineering, Obninsk, Kaluga-Region, Russia

The neutron capture cross sections of ^{175}Lu and ^{176}Lu have been measured in the energy range 3–225 keV at the Karlsruhe 3.7 MV Van de Graaff accelerator. Neutrons were produced via the ^{7}Li$(p, n)^7$Be reaction by bombarding metallic Li targets with a pulsed proton beam, and capture events were registered with the Karlsruhe 4π barium fluoride detector. The cross sections were determined relative to the gold standard using isotopically enriched as well as natural lutetium oxide samples. Overall uncertainties of $\sim$1% could be achieved in the final cross section ratios to the gold standard, about a factor of 5 smaller than in previous works. Maxwellian averaged neutron capture cross sections were calculated for thermal energies between $kT = 8$ and 100 keV. These values are systematically larger by $\sim$7% than those reported in recent evaluations. These results are of crucial importance for the assessment of the s-process branchings at $A = 175/176$.

I. INTRODUCTION

One of the prime motivations for the construction of the Karlsruhe 4π BaF$_2$ detector nearly 20 years ago was the verification of the σN Systematics [1], the genuine characteristics of nucleosynthesis in the slow neutron capture process (or *s* process for short). The validity of the *s*-process concept, which is related to the He-burning zones in Red Giant stars, implies that the product of the abundances N_s produced in the *s* process and neutron capture cross section $\langle\sigma\rangle$ averaged over the thermal stellar spectrum is a smooth function of mass number. In mass regions between magic neutron numbers, this function is expected to exhibit an almost constant dependence on mass number, a behavior that corresponds to reaction flow equilibrium. This *local* equilibrium can best be tested in the mass region of the rare earth elements (REE). Due to the close chemical similarity of the REE in the solar system, their relative abundances are very accurately defined by analyses of a certain class of meteorites, the so-called carbonaceous chondrites [2]. In fact, the 14 REE abundances are known with relative uncertainties of $\approx$1.7%, whereas the majority of the elemental abundances carry uncertainties of 5–10%.

The REE comprise 55 stable isotopes with 40 being situated on the reaction path of *s*-process nucleosynthesis. Among the remaining cases, seven stable isotopes can be ascribed exclusively to the *r* process and eight to the *p* process, which are both related to explosive nucleosynthesis in supernovae. The present experiment with the Karlsruhe 4π BaF$_2$ detector has determined the stellar neutron capture cross sections of 29 of the 40 isotopes on the *s*-process path, including seven of the eight *s*-only isotopes in this mass region. The 1% accuracy that can be achieved with this detector matches the 1.7% uncertainty of the REE abundances, thus providing the most crucial test of the σN systematics.

Nine of the remaining 11 isotopes are accessible to the activation technique, which was shown to yield similar uncertainties. Indeed, several of these cases have been measured recently by activation [3–5].

The *s*-process reaction path in the vicinity of lutetium is sketched in Fig. 1. Lutetium is the last REE and is followed by the element hafnium. Due to its long half-life of 36 Gyr, this isotope was initially considered as a potential nuclear chronometer for the age of the *s* elements. This possibility is based on the fact that ^{176}Lu as well as its daughter ^{176}Hf are of pure *s*-process origin since they are both shielded against the *r*-process β decay chains by their stable isobar ^{176}Yb. However, it was found that the thermal photon bath at typical *s*-process temperatures is energetic enough for induced transitions from the long-lived ground state to the short-lived isomer ($t_{1/2} = 3.68$ h), thus dramatically reducing the effective half-life to a few hours. This effect changes the information contained in the ^{176}Lu/^{176}Hf pair from a potential chronometer into a sensitive *s*-process thermometer [6–8].

Due to its importance to *s*-process studies, lutetium has attracted considerable scientific interest. For ^{175}Lu, a set of five time-of-flight (TOF) measurements of the neutron capture cross section in the relevant keV region are listed in the compilation of Bao *et al.* [9]. These experiments were facilitated by the 97.4% natural abundance of ^{175}Lu, which does not require enriched sample material. The results of four measurements between 1972 and 1984 were consistent within the quoted uncertainties of 4%–15%. However, the most recent measurement by Bokhovko *et al.* [10] reported a much smaller cross section, incompatible with the previous data. For ^{176}Lu, the low natural abundance requires enriched samples. These measurements were difficult since the available enrichment was limited to $\approx$72% and implied considerable corrections for isotopic impurities. Though the results of Beer *et al.* [11], which were obtained in experiments at two different accelerators, agreed within the quoted uncertainties of $\approx$5%, these data differed significantly from the earlier

---

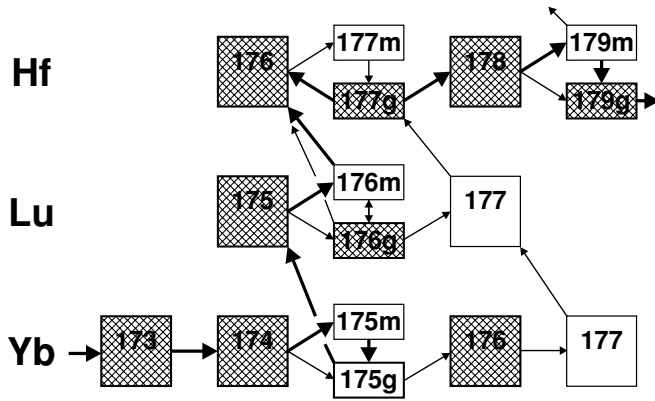*Electronic address: franz.kaeppeler@ik.fzk.de

FIG. 1. Reaction network of the *s* process in the region of the lutetium isotopes formed by neutron capture reactions (arrows to the right) and subsequent β decays (arrows to the next higher elements). Stable and radioactive isotopes are plotted as shaded and open boxes, respectively. Important isomeric states are indicated by separate boxes. All isomers are depopulated to the respective ground states before capturing a neutron, except in case of ^{176}Lu, where the isomer can be significantly populated (see text). Note that ^{176}Lu and ^{176}Hf represent *s*-only isotopes since they are shielded against β decays from the *r*-process region by ^{176}Yb.

TOF measurements of Shorin *et al*. [12] and Macklin and Gibbons [13] as well as from activation measurements of Beer and Käppeler [14].

In the present experiment, a natural as well as a highly enriched sample was used to measure the neutron capture cross section of ^{175}Lu. In the case of the less enriched ^{176}Lu sample, the necessary correction for isotopic impurities could be performed with significantly improved accuracy, taking advantage of the good resolution in γ-ray energy of the Karlsruhe 4π BaF$_2$ detector.

Measurements and data analysis are described in Secs. II and III, followed by a discussion of the results and uncertainties in Secs. IV and V. The stellar cross sections are presented in Sec. VI. The astrophysical implications are briefly addressed in Sec. VII. A detailed description of the technical part, including data evaluation methods, calculation of correction factors, and the results from individual experimental runs, can be found in Ref. [15].

II. EXPERIMENT

The neutron capture cross sections of the two stable lutetium isotopes 175 and 176 have been measured in the energy range of 3–225 keV using gold as a standard. Since the experimental method has been published in detail [16,17], only a general description is given here, complemented with the specific features of the present measurement.

Neutrons were produced via the ^{7}Li$(p, n)^7$Be reaction by bombarding metallic Li targets with the pulsed proton beam of the Karlsruhe 3.7 MV Van de Graaff accelerator. The neutron energy was determined by time of flight, the samples being located at a flight path of 79 cm. The relevant parameters of the accelerator were a pulse width of $<$1 ns, a repetition rate of 250 kHz, and an average beam current of 2.0 μA. In different runs, the proton energy was adjusted to 30 and 100 keV above the threshold of the ^{7}Li$(p, n)^7$Be reaction at 1.881 MeV. In this way, continuous neutron spectra in the proper energy range for *s*-process studies were obtained, ranging from 3 to 100 keV, and 3 to 225 keV, respectively. The lower maximum neutron energy offers a significantly better signal-to-background ratio at lower energies.

Capture events were registered with the Karlsruhe 4π barium fluoride detector via the prompt capture γ-ray cascades. This detector consists of 42 hexagonal and pentagonal crystals forming a spherical shell of BaF$_2$ with 10 cm inner radius and 15 cm thickness. It is characterized by a resolution in γ-ray energy of 7% at 2.5 MeV, a time resolution of 500 ps, and a peak efficiency of 90% at 1 MeV. The 1.7 MeV threshold in γ-ray energy used in the present experiment corresponds to an efficiency for capture events of more than 95% for all investigated isotopes. A comprehensive description of the detector can be found in Ref. [18].

The experiment was divided into three runs, two using the conventional data acquisition technique with the detector operated as a calorimeter, and a third with an analog-to-digital converter (ADC) system coupled to the detector for analyzing the signals from all modules individually. In this way, the full spectroscopic information recorded by the detector could be recovered.

The lutetium samples were prepared from isotopically enriched oxide powder (Lu$_2$O$_3$), which was heated to 1200 K for 15 min to eliminate any water contamination. Then the oxide was pulverized in an agate mortar, pressed into pellets 15 mm in diameter, and reheated to 1200 K for 1 h. During the final heating, the pellets shrank slightly. Immediately after cooling, the actual samples were prepared by canning the pellets into airtight aluminum cylinders with 0.2 mm thick walls. Apart from the two lutetium samples, a gold sample in an identical can was used for measuring the neutron flux, and an empty can served for determining the sample-independent background. The background due to scattered neutrons was measured by means of a graphite sample. The relevant sample parameters and the isotopic composition of the lutetium samples are compiled in Tables I and II. In the last run of the experiment, the enriched ^{175}Lu sample was replaced by a sample made of natural lutetium oxide.

The measured spectra of all samples were normalized to equal neutron flux by means of a ^{6}Li glass monitor located close to the neutron target. The transmission spectra measured with a second ^{6}Li glass detector at a flight path of 260 cm were used for a rough determination of the total cross sections. Though the accuracy of this method is inferior to that obtained in a dedicated experiment, these total cross sections are adequate for calculating the multiple scattering corrections.

The samples were moved cyclically into the measuring position by a computer-controlled sample changer. The data acquisition time per sample was about 10 min, a complete cycle lasting about 0.8 h. From each event, a 64 bit word was recorded containing the sum energy and TOF information together with 42 bits identifying the contributing detector modules. The respective parameters of the three runs corresponding to neutron spectra with different maximum energies are listed in Ref. [15]. The total measuring time was $\sim$22 d.

TABLE I. Sample characteristics.

Sample	Diameter (mm)	Thickness		Weight (g)	Can[b] (g)	Neutron separation energy (MeV)
		(mm)	(10^{-3}at/b)[a]			
Graphite[c]	15.0	2.0	17.628	0.6213	0.187	–
^{176}Lu	15.0	1.8	3.4139	2.0008	0.318	7.073
^{197}Au	15.0	0.4	2.2485	1.2996	0.258	6.513
^{175}Lu	14.6	0.9	1.1943	0.6974	0.244	6.293
Empty[c]	15.0	–	–	–	0.278	–
^{nat}Lu[d]	14.4	1.3	1.7212	1.0052	0.251	–

[a]For lutetium samples: sum of all Lu isotopes.
[b]Aluminum cylinder.
[c]Corresponding to sample order of runs I and II. In run III, the positions of the graphite sample and the empty can were exchanged.
[d]In run III, the natural lutetium sample was used instead of the enriched ^{175}Lu.

III. DATA ANALYSIS

A. Total cross sections

The total cross sections of the investigated isotopes were determined in the neutron energy range of 10–200 keV via the TOF spectra measured with the ^{6}Li glass detector at a flight path of 260 cm. The total cross sections and related uncertainties were obtained as described in Ref. [16] and are listed in Table III. Apart from the energy bins, which are affected by strong scattering resonances of the aluminum sample cans, the carbon cross sections agree with the data from the JEFF-3.1 evaluated data library [19] within $\pm5.0\%$.

The quoted uncertainties were obtained under the assumption that they are inversely proportional to the fraction of neutrons interacting in the sample, $A = 1 - T$, where T is the transmission. For the carbon sample this fraction is $A = 7.2\%$, the related uncertainty of 5.0% being estimated from the comparison with the JEFF data. The graphite and gold samples had also been used in similar experiments on hafnium isotopes [20]. The results for the carbon cross sections of both experiments agree to better than 0.3% and for the gold cross sections to better than 0.7%, confirming the good reproducibility of the method.

In the energy range of 10–100 keV, no other experimental data were found in the literature. The results for both lutetium isotopes agree within the quoted uncertainties with the two evaluated nuclear data files JEFF-3.1 and ENDF-B/VI, which also indicate that the total cross sections depend weakly on neutron energy.

B. Capture cross sections

The analysis was carried out in the same way as described previously [16,17]. All events were sorted into two-dimensional spectra containing 128 sum-energy versus 2048 TOF channels according to different multiplicities (evaluation 1). In evaluation 2, this procedure was repeated by rejecting those events in which only neighboring detector modules contributed to the sum-energy signal. With this option, background from the natural radioactivity of the BaF$_2$ crystals and from scattered neutrons could be reduced. For all samples, the resulting spectra were normalized to equal neutron flux using the count rate of the ^{6}Li glass monitor close to the neutron target. The corresponding normalization factors are below 0.5% for all runs. The treatment of the two-dimensional spectra from the data recorded with the ADC system is slightly more complicated and was performed as described in Ref. [16].

In the second step of data analysis, sample-independent backgrounds were removed by subtracting the spectra measured with the empty can. A remaining constant background was determined at very long flight times, in which no time-correlated events are expected.

TABLE II. Isotopic composition (%).

Sample	Isotope	
	^{175}Lu	^{176}Lu
^{175}Lu	99.50	0.50
^{176}Lu	27.54	72.46
^{nat}Lu	97.41	2.59

TABLE III. Measured total cross sections (determined from the count rate of the ^{6}Li glass neutron monitor at 260 cm flight path).

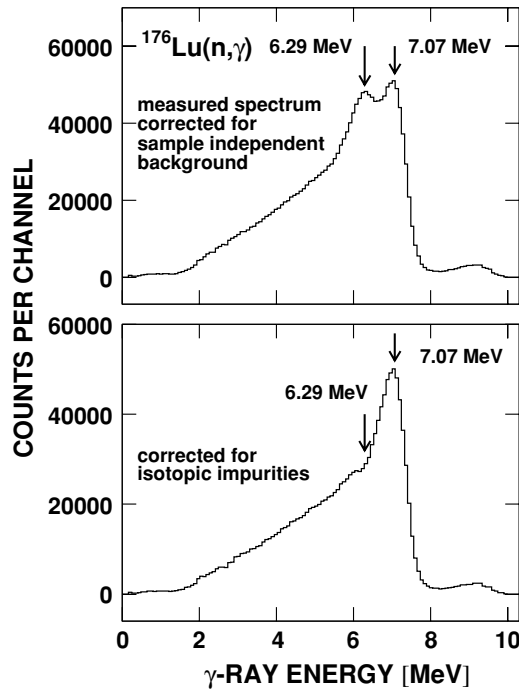| Neutron energy (keV)	Total cross section (b)			
	^{175}Lu	^{176}Lu	^{12}C	^{197}Au
10–15	10.3	13.1	3.99	13.1
15–20	11.5	12.7	4.16	13.6
20–30	12.3	12.5	4.47	13.7
30–40	10.3	11.8	3.71	11.9
40–60	10.2	11.6	4.39	12.1
60–80	10.6	12.7	4.32	11.3
80–100	10.3	10.2	3.82	10.6
100–150	10.7	8.7	3.94	8.3
150–200	11.5	8.6	3.87	7.4
Typical uncertainty (%)	24	9	5	12

FIG. 2. Sum-energy spectra of the [176]Lu sample. The correction of isotopic impurities according to the isotopic matrix does not result in a dip at the position of the binding energy of [175]Lu (6.29 MeV), indicating an overcompensation as observed for a [176]Hf sample of compatibly low enrichment [20].
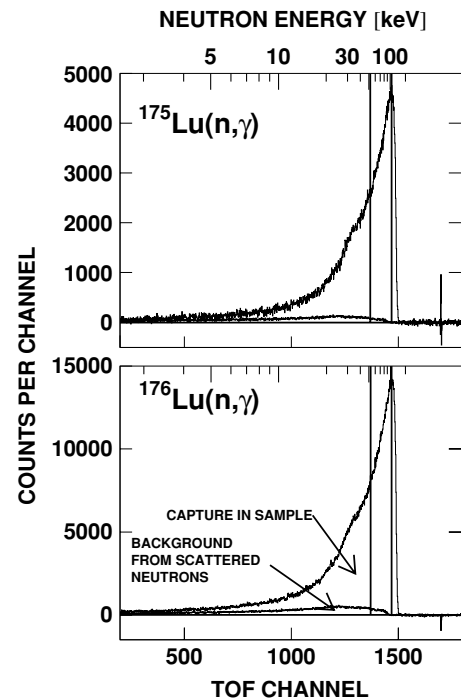

FIG. 3. TOF spectra measured with both Lu samples in run I (100 keV maximum neutron energy). Background due to sample scattered neutrons is shown separately. Two vertical lines indicate the region used for absolute normalization of the cross section.

At this point, the spectra contain only events correlated with the sample. The next correction to be made is for isotopic impurities (see Ref. [16] for details). The respective coefficients are compiled in Ref. [15]. Because of the comparably low enrichment of the [176]Lu sample, the correction is about 20% of the measured effect, while it is nearly negligible for the highly enriched [175]Lu sample.

As discussed in Ref. [21], the present method to correct for isotopic impurities holds exactly only if all samples are about equal in weight since only then are second-order effects due to neutron multiple scattering and self-absorption properly accounted for. In the present experiment, the largest correction is required for the [176]Lu sample because of the [175]Lu admixture of 27.5%. The weights of the two samples differ by a factor of 2.8. Calculating the correction directly from the isotopic matrix may, therefore, lead to an overcompensation due to the smaller self-shielding effect in the thinner [175]Lu sample. With the good energy resolution of the 4π BaF$_2$ this effect can be checked in the corrected sum-energy spectrum of [176]Lu, where this effect would cause a dip at the neutron separation energy of [175]Lu at 6.29 MeV. In contrast to a recent measurement on [176]Hf [20], this effect is not observed in the present case (Fig. 2).

Following the correction for isotopic impurities, the background due to capture of sample scattered neutrons was removed from the spectra by means of the data measured with the scattering sample. The binding energy of both lutetium isotopes is low enough that the correction can be normalized using the pronounced peak in the sum-energy spectra at

9.1 MeV due to capture in the odd barium isotopes [135]Ba and [137]Ba. After this last correction, the final spectra contain only the net capture events of the investigated isotopes. The corrections for capture of scattered neutrons are shown for both measured Lu isotopes in Fig. 3.

After subtraction of the scattering background, the cross section shape versus neutron energy was determined from the TOF spectra of Fig. 3. These spectra are calculated by integrating the two-dimensional spectra in a region around the full energy peak. Because of the different background conditions in the spectra of events with different multiplicities, this range was chosen to decrease with multiplicity (see Fig. 5). For normalization, the two-dimensional data were projected onto the sum-energy axis using the TOF region with optimum signal-to-background ratio as indicated in Fig. 3 by two vertical lines. The resulting pulse height spectra are shown in Fig. 4 for events with multiplicity >2. The threshold in sum energy is 1.7 MeV.

The sum-energy spectra of both Lu isotopes are shown in Fig. 5 for different multiplicities. These multiplicities correspond to the number of detector modules contributing per event and are slightly larger than the true multiplicities because of cross talking. The arrows in Fig. 5 indicate the range of sum-energy channels that were integrated to obtain the TOF spectra of Fig. 3 for determining the cross section shapes.

The cross section ratio of isotope X relative to the gold standard is given by

$$\frac{\sigma_i(X)}{\sigma_i(Au)} = \frac{Z_i(X)}{Z_i(Au)} \frac{\Sigma Z(Au)}{\Sigma Z(X)} \frac{\Sigma E(X)}{\Sigma E(Au)} \frac{m(Au)}{m(X)} F_1 F_2. \quad (1)$$
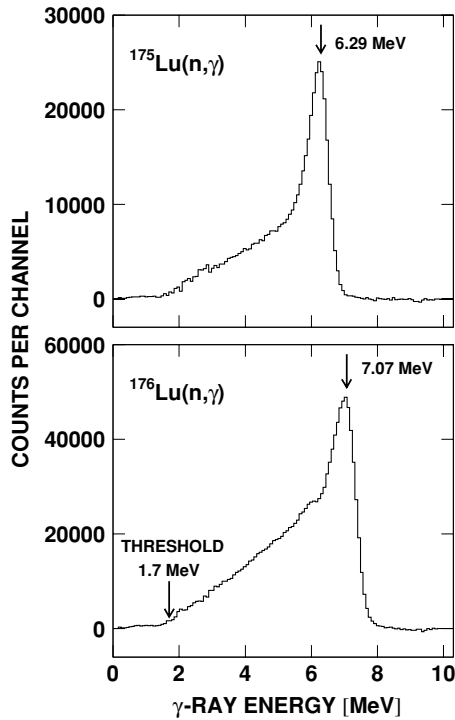
FIG. 4. Sum-energy spectra measured in run I containing events with multiplicity >2. These spectra were obtained by projection of the two-dimensional spectra in the TOF region below the maximum neutron energy as indicated by vertical lines in Fig. 3.
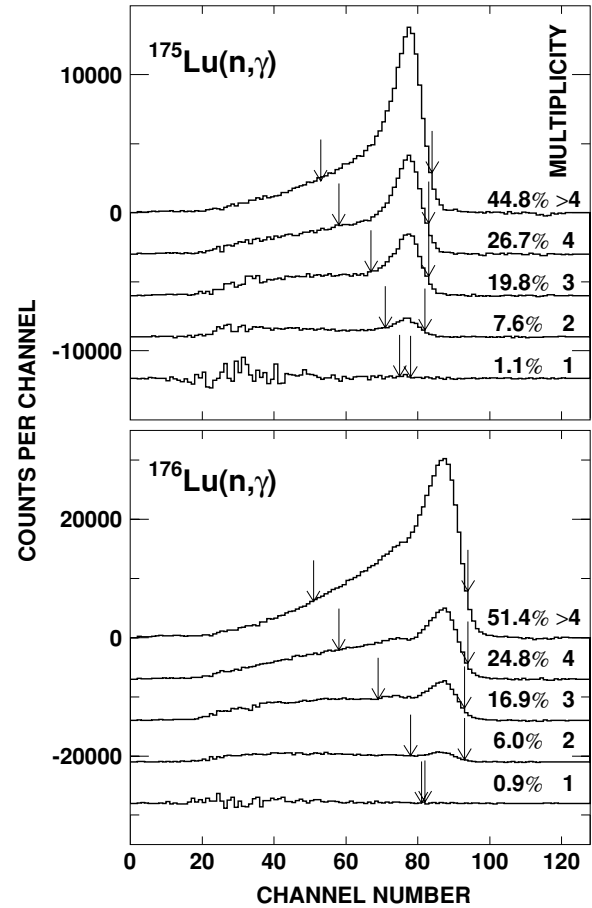

FIG. 5. Sum-energy spectra as a function of multiplicity. Arrows indicate the regions integrated to determine the cross section shape (see TOF spectra of Fig. 3).

In this expression, Z_i is the count rate of channel i in the TOF spectrum, ΣZ is the TOF rate integrated over the interval used for normalization (vertical lines in Fig. 3), ΣE is the total count rate in the sum-energy spectra for all multiplicities, in this TOF interval. The respective sum-energy spectra are shown in Fig. 5. For all multiplicities, these spectra were integrated from the threshold at 1.7 MeV beyond the binding energy, and the sum of these results ΣE is used in Eq. (1). A full description of this procedure is given in Ref. [22]. The quantity m is the sample thickness in atoms/barn. The factor $F_1 = [100 - f(Au)]/[100 - f(X)]$ corrects for the fraction of capture events f below the experimental threshold in sum energy, where X refers to the respective lutetium sample (Table IV); and F_2 is the ratio of the multiple scattering and self-shielding corrections.

The fraction of unobserved capture events f and the correction factor F_1 were calculated as described in Ref. [23]. The input for this calculation are the individual neutron capture cascades and their relative contributions to the total capture cross section as well as the detector efficiency for monoenergetic γ rays in the energy range up to 10 MeV. As in the experiment on dysprosium isotopes [24], this information was derived directly from the experimental data recorded with the ADC system in run III. From these data, only events close to the sum-energy peak (see Fig. 4) were selected, which contained the full capture γ-ray cascade. This ensemble was further reduced by restricting the analysis to the TOF region with optimum signal-to-background ratio (vertical lines in Fig. 3). The correction factors F_1 are quoted in Table IV.

The corrections for neutron multiple scattering and self-shielding were calculated with the SESH code [25]. Apart from the pairing energies [26], most of the input parameters were taken from Ref. [27], but were slightly modified in order to reproduce the measured total and capture cross sections. For the ^{175}Lu sample, it was difficult to find adequate parameters that reproduced the experimentally observed flat shape of the total cross section (see Table III). The final values are listed in Ref. [15] together with the calculated total cross sections as well as the resulting correction factors, MS(X) and F_2. In general, these corrections are smaller than 2%.

IV. DIFFERENTIAL NEUTRON CAPTURE CROSS SECTIONS

The measured neutron capture cross section ratios of the investigated Lu isotopes and of ^{197}Au are listed in Ref. [15] together with the respective statistical uncertainties. The data are given for all runs and for the two evaluation methods discussed in Sec. III. The data are free of systematic differences with respect to the various runs and evaluations and well consistent within the quoted statistical uncertainties. This holds also for the ^{175}Lu results, which were obtained with enriched and natural samples.

TABLE IV. Fraction of undetected capture events f (%) and the related correction factors F_1 (derived from capture cascades measured with the ADC system).

	Threshold in sum energy (MeV)		
	1.5	1.7	2.0
f(Au)	5.15	–	7.09
f(175Lu)	3.06	–	4.65
f(176Lu)	1.99	–	3.15
F_1(175Lu/Au)	0.978	0.977	0.974
F_1(176Lu/Au)	0.968	0.964	0.959

As in previous studies with the 4π BaF$_2$ detector [16,17,28], the final cross section ratios were adopted from evaluation 2. The respective mean values are compiled in Table V together with the statistical, systematic, and total uncertainties. The energy bins are sufficiently fine to avoid systematic effects in calculating the Maxwellian averaged cross sections (Sec. VI). Statistical uncertainties below 1.0% could be obtained in the energy bins from 15 to 200 keV. The systematic uncertainties range between 0.7% and 0.8%.

The experimental ratios were converted into absolute cross sections using the gold data of Macklin [29] after normalization by a factor of 0.989 to the absolute value of Ratynski and Käppeler [30] (Table VI). The uncertainties of the resulting values can be obtained by adding the 1.5% uncertainty of the reference cross section to the uncertainties of the respective cross section ratios.

TABLE VI. Neutron capture cross sections of 175Lu and 176Lu (in mb).

Energy bin[a] (keV)	σ(197Au)[b]	σ(175Lu)	σ(176Lu)
3–5	2266.7	4209	5545
5–7.5	1726.7	3024	4190
7.5–10	1215.7	2475	3411
10–12.5	1066.7	1981	2677
12.5–15	878.0	1787	2435
15–20	738.8	1587	2111
20–25	600.0	1364	1837
25–30	570.8	1230	1665
30–40	500.4	1079	1434
40–50	433.3	977.2	1274
50–60	389.6	866.3	1155
60–80	349.4	772.1	1028
80–100	298.3	678.0	897.0
100–120	290.1	635.9	862.8
120–150	274.1	559.1	830.9
150–175	263.7	512.4	800.8
175–200	252.6	478.9	749.8
200–225	248.5	464.6	722.3

[a]As used for calculating the Maxwellian averaged cross sections.
[b]Based on the 197Au data discussed in text.

V. DISCUSSION OF UNCERTAINTIES

The determination of statistical and systematic uncertainties followed the procedures applied in previous measurements with the 4π BaF$_2$ detector [16,17]. Therefore, a discussion of the particular aspects of the present experiment may suffice

TABLE V. Final neutron capture cross section ratios of 175Lu and 176Lu relative to 197Au. Abbreviations refer to statistical, systematic, and total uncertainties.

Energy bin[a] (keV)	$\dfrac{\sigma(^{175}\text{Lu})}{\sigma(^{197}\text{Au})}$	Uncertainty (%)			$\dfrac{\sigma(^{176}\text{Lu})}{\sigma(^{197}\text{Au})}$	Uncertainty (%)		
		stat	sys	tot		stat	sys	tot
3–5	1.8569	4.3	0.7	4.4	2.4463	3.9	0.8	4.0
5–7.5	1.7513	2.6	0.7	2.7	2.4264	2.3	0.8	2.4
7.5–10	2.0354	2.1	0.7	2.2	2.8057	1.9	0.8	2.1
10–12.5	1.8575	1.6	0.7	1.7	2.5093	1.4	0.8	1.6
12.5–15	2.0356	1.4	0.7	1.6	2.7729	1.3	0.8	1.5
15–20	2.1478	0.9	0.7	1.1	2.8571	0.8	0.8	1.1
20–25	2.2732	0.8	0.7	1.1	3.0611	0.7	0.8	1.1
25–30	2.1538	0.6	0.7	0.9	2.9176	0.6	0.8	1.0
30–40	2.1558	0.5	0.7	0.9	2.8651	0.4	0.8	0.9
40–50	2.2551	0.5	0.7	0.9	2.9390	0.4	0.8	0.9
50–60	2.2234	0.5	0.7	0.9	2.9634	0.4	0.8	0.9
60–80	2.2101	0.4	0.7	0.8	2.9435	0.4	0.8	0.9
80–100	2.2728	0.4	0.7	0.8	3.0071	0.4	0.8	0.9
100–120	2.1917	0.4	0.7	0.8	2.9738	0.4	0.8	0.9
120–150	2.0394	0.8	0.7	1.1	3.0312	0.6	0.8	1.0
150–175	1.9435	0.8	0.7	1.1	3.0373	0.7	0.8	1.1
175–200	1.8961	0.9	0.7	1.1	2.9686	0.8	0.8	1.1
200–225	1.8699	1.3	0.7	1.5	2.9070	1.1	0.8	1.4

[a]Energy bins as used for calculating the Maxwellian averaged cross sections.

TABLE VII. Systematic uncertainties (%).

Flight path	0.1
Neutron flux normalization	0.2
Sample mass: elemental impurities	0.2
Isotopic composition (^{175}Lu/ ^{176}Lu)	0.2/0.3
Isotopic correction (^{175}Lu/ ^{176}Lu)	0.2/0.4
Multiple scattering and self-shielding: F_2	
Cross section ratio	0.4
Undetected events: F_1	
Cross section ratio	0.4
Total systematic uncertainties	
$\sigma(^{175}$Lu$)/\sigma($Au$)$	0.7
$\sigma(^{176}$Lu$)/\sigma($Au$)$	0.8

here. The various contributions to the overall uncertainties are compiled in Table VII.

The binding energy for both lutetium isotopes is sufficiently low that the scattering background could be normalized in the sum-energy region around 9 MeV. Therefore, no systematic differences were observed in the data, neither between individual runs nor correlated with the different acquisition modes or evaluation methods. Accordingly, systematic uncertainties in background subtraction were negligible as in the measurements on the samarium [16], gadolinium [21], and dysprosium [24] isotopes.

The minor systematic uncertainties related to the flight path measurement and the neutron flux normalization have been discussed previously.

The enriched samples contained several impurities at the level of about 50 ppm, but the total contamination was less than 0.06% in both cases. For the natural sample, this contamination was below 6 ppm. The rare earth contamination consisted only of ytterbium, which contributed less than 0.2% to the enriched sample and 50 ppm to the natural sample. Since the capture cross sections of the impurities were smaller than or compatible with those of the Lu isotopes, a systematic uncertainty of 0.2% was sufficient to account for the impurities.

The isotopic composition was specified with absolute uncertainties between 0.1% and 0.2% (Table II). Though these seem to be rather conservative numbers [31], they were adopted in the data analysis, resulting in relative uncertainties of 0.2% and 0.3% for the mass of the main isotopes in the ^{175}Lu and ^{176}Lu sample, respectively.

The uncertainty related to the isotopic correction has been discussed in detail elsewhere [21,24]. For the rather large correction required for the ^{176}Lu sample, this uncertainty can be evaluated from the spectra in Fig. 2. In the evaluated energy range from threshold up to 7.7 MeV, the count rate in the upper spectrum consists of contributions from captures in ^{176}Lu (76.5%) and in ^{175}Lu (21.8%), and from capture from scattered neutrons (1.7%). If the absolute uncertainty of 0.2% for the main isotope and for ^{175}Lu is taken into account, the impurity correction implies an uncertainty of 0.4%. For the ^{175}Lu and natural lutetium samples, the small isotopic corrections give an uncertainty of 0.2% at most.

Samples with low enrichment are also problematic with respect to the correction for multiple scattering and self-

shielding. Subtraction of the normalized spectra of the impurity isotopes may be insufficient or may even overcompensate for the multiple scattering effect. This certainly holds if the individual sample masses are significantly different as in the case of ^{176}Lu. For the ^{176}Lu sample, the effect is not visible in the spectra but may still cause a small uncertainty. Therefore, the calculation of the correction factors MS was performed twice, before and after the correction for isotopic impurities. The respective difference is 1.0% for the ^{176}Lu sample, nearly independent of neutron energy. In analogy to the gadolinium and dysprosium experiments [21,24], 25% of this difference was adopted as an additional uncertainty and added to the uncertainty provided by the SESH code [25]. For the ^{175}Lu sample, this effect is negligible because of the high enrichment.

The detailed discussion of the systematic uncertainties due to undetected events for the gadolinium experiment [21] showed that uncertainties of the correction factor F_1 were 0.3% for the even and 0.8% for the odd isotopes. These corrections were based on two independent sets of calculated capture cascades and were found to agree with the respective uncertainties quoted in previous measurements with the 4π BaF$_2$ detector [16,17,28]. It turned out that this uncertainty was mainly determined by the difference in neutron separation energy between the investigated isotope and the gold standard, which is large for the odd, but small for the even gadolinium isotopes. This behavior is consistent with the corrections found for various dysprosium isotopes [24], thus confirming the reliability of the evaluated uncertainties. With this procedure, an uncertainty of 0.4% was assigned for the two lutetium isotopes.

VI. MAXWELLIAN AVERAGED CROSS SECTIONS

Maxwellian averaged cross sections were calculated in the same way as described in Refs. [17,23]. The neutron energy range from thermal to 700 keV was divided into three intervals I_x according to the origin of the adopted cross sections (see Ref. [15]). The dominant part I_2 between 3 and 225 keV is provided by the present experiment (Table VI). These data were obtained with sufficient resolution in neutron energy to exclude systematic uncertainties in the calculation of the Maxwellian averages.

The contribution I_1 was determined by normalizing the cross sections of Kopecky *et al.* [32] to the present data in the interval between 3 and 10 keV. Since the shape of both data sets were found in good agreement, an uncertainty of 5% was assumed for the contribution I_1.

At typical *s*-process temperatures, the energy interval from 225 to 700 keV contributes very little to the Maxwellian average. For this part, the data of Kopecky *et al.* [32] were normalized to the present results between 50 and 225 keV, and the corresponding uncertainties were assumed to increase from 2% at 225 keV to 10% at 700 keV. The results are compiled in Table VIII.

The systematic uncertainties of the Maxwellian averaged cross sections are determined by the uncertainties of the measured cross section ratios in the interval I_2 as well as by the respective I_1 and I_3 contributions. The 1.5% uncertainty

TABLE VIII. Maxwellian averaged (n, γ) cross sections of ^{175}Lu and ^{176}Lu.

Isotope	kT (keV)	I_1 (0–3 keV) (mb) Ref. [32]a	I_2 (3–225 keV) (mb) This work	I_3 (225–700 keV) (mb) Ref. [32]a	$\langle \sigma v \rangle / v_T$ (mb)	stat	sysb	tot
^{175}Lu	8	508 ± 25	2153 ± 21	0.0	2661	33	31	45
	10	339 ± 17	1970 ± 16	0.0	2309	23	23	33
	15	160 ± 8	1643 ± 10	0.0	1802	13	15	20
	20	91.9 ± 4.6	1433 ± 7	0.1	1525	8.3	12	15
	25	59.8 ± 3.0	1286 ± 5	0.4	1346	6.2	10	12
	30	42.0 ± 2.1	1175 ± 5	1.5	1219	5.0	8.8	10
	40	23.9 ± 1.2	1012 ± 4	7.5 ± 0.2	1043	3.7	7.4	8
	50	15.5 ± 0.8	890 ± 3	18.5 ± 0.5	924	3.0	6.5	7
	52	14.3 ± 0.7	869 ± 3	21.2 ± 0.6	904	2.9	6.3	7
	60	10.8 ± 0.5	790 ± 3	32.6 ± 1.0	834	2.8	5.8	6
	70	8.0 ± 0.4	705 ± 2	47.6 ± 1.5	761	2.8	5.3	6
	80	6.1 ± 0.3	632 ± 2	62.0 ± 2.1	701	3.0	4.9	6
	90	4.8 ± 0.2	569 ± 2	75.1 ± 2.7	649	3.3	4.5	6
	100	3.9 ± 0.2	514 ± 2	86.3 ± 3.2	604	3.7	4.2	6
^{176}Lu	8	675 ± 34	2911 ± 25	0.0	3586	42	45	62
	10	450 ± 22	2659 ± 19	0.0	3109	29	33	44
	15	211 ± 11	2210 ± 12	0.0	2421	16	22	27
	20	122 ± 6	1924 ± 8	0.1	2046	10	17	20
	25	79.5 ± 4.0	1726 ± 6	0.6	1806	7.5	15	17
	30	55.8 ± 2.8	1581 ± 5	2.3 ± 0.1	1639	6.0	13	14
	40	31.8 ± 1.6	1371 ± 4	11.1 ± 0.3	1414	4.4	11	12
	50	20.6 ± 1.0	1216 ± 4	27.2 ± 0.8	1264	3.7	10	11
	52	19.0 ± 1.0	1189 ± 3	31.1 ± 0.9	1239	3.7	9.9	11
	60	14.4 ± 0.7	1088 ± 3	47.9 ± 1.5	1150	3.5	9.2	10
	70	10.6 ± 0.5	978 ± 3	69.9 ± 2.3	1059	3.7	8.5	9
	80	8.1 ± 0.4	882 ± 3	91.2 ± 3.1	981	4.1	7.8	9
	90	6.4 ± 0.3	797 ± 2	110.3 ± 3.9	914	4.6	7.3	9
	100	5.2 ± 0.3	723 ± 2	126.8 ± 4.6	855	5.1	6.8	9

aNormalized to present data.

bThe 1.5% uncertainty of the gold standard is not included, since it cancels out in most applications of relevance to astrophysics.

of the gold standard was not included since it cancels out in most applications of relevance for s-process studies. In general, the systematic uncertainties dominate over the statistical uncertainties, except at low thermal energies.

The present results at $kT = 30$ keV are eventually compared in Table IX with previous experiments and with the compilations of Bao et al. [9] and of Beer, Voss, and Winters [33]. For ^{175}Lu, good agreement is found with the four older measurements. In fact, the present value agrees to better than 1% with the average of these four data sets, whereas the more recent value based on the measurement of Bokhovko et al. [10] is significantly smaller. For the astrophysical discussion, the isomeric ratio

$$\mathrm{IR} = \frac{\text{partial } (n, \gamma) \text{ cross section to isomer}}{\text{total } (n, \gamma) \text{ cross section}}$$

is important since it determines the shortcut of the reaction flow to ^{176}Hf via the decay of the 3.68 h isomer in ^{176}Lu. Combined with the partial cross section of Zhao and Käppeler [34] measured for a thermal spectrum corresponding to $kT = 25$ keV, the present results yield IR = 0.843 ± 0.023, which

is significantly smaller than the value of 0.90 ± 0.05 obtained so far [9].

The present result for the (n, γ) cross section of ^{176}Lu is larger than the TOF measurements by Beer et al. [11], which were performed at different accelerators, while it agrees with the activation measurement of Beer and Käppeler [14]. This comparison may reflect problems with the large correction for isotopic impurities that affects only the TOF measurement. Consequently, the present data are systematically larger by ∼7% compared to recent evaluations [9,33] and exhibit five times smaller uncertainties.

VII. ASTROPHYSICAL IMPLICATIONS

The accurate cross sections reported here constitute an essential part of the nuclear input for a comprehensive analysis of branching at $A = 176$ since they determine the production and destruction of ^{176}Lu. Determination of the remaining cross section information has recently been completed by performing parallel measurements of the ^{176}Hf cross section

TABLE IX. Maxwellian averaged (n, γ) cross sections (in mb) at $kT = 30$ keV compared to previous experiments and evaluations.

Isotope	Experiment		Evaluation	
	Cross section (mb)	Reference	Bao et al. [9]	Beer, Voss, Winters [33]
[175]Lu	1219 ± 10	This work[a]	1146 ± 44	1179 ± 44
	992 ± 50	Bokhovko et al. (92) [10]		
	1179 ± 44	Beer et al. (84) [11]		
	1266 ± 43	Beer et al. (81) [6]		
	1206 ± 54	Macklin et al. (78) [36]		
	1265 ± 190	Lepine et al. (72) [37]		
[176]Lu	1639 ± 14	This work[a]	1532 ± 69	1537 ± 60
	1526 ± 69	Beer et al. (84) [11]		
	1514 ± 56	Beer et al. (84) [11]		
	1718 ± 85	Beer et al. (80) [14]		
	2236 ± 335	Shorin et al. (73) [12]		

[a] The 1.5% uncertainty of the gold cross section is not included, since it cancels out in most applications of relevance for nuclear astrophysics.

[20] and the partial cross section of [175]Lu at a thermal energy $kT = 5$ keV [35].

Qualitatively, the present results suggest that both the production and destruction cross sections of the long-lived ground state [176]Lu^g are larger than previously assumed. This simple argument is challenged, however, by the strong temperature dependence of the [176]Lu half-life at the high temperatures reached during stellar He burning [7,8]. It was shown that interactions with the hot stellar photon bath via thermally induced transitions result in a coupling between ground state and isomer. The consequences of this coupling change with temperature in the following way:

(i) Below 150 million K, the reaction path of Fig. 1 is completely defined by the partial capture cross sections feeding ground state and isomer in [176]Lu. Internal transitions are far too weak and have negligible effect on the branching.

(ii) Between 240 and 300 million K thermally induced transitions cause drastic changes in the population probabilities of ground state and isomer, resulting in an enhanced feeding of the ground state. It is due to this effect that more [176]Lu is observed in nature than would be created in a "cool" environment. In this regime, internal transitions, β decays, and neutron captures are equally important.

(iii) For temperatures above 300 million K thermal equilibrium in the relative population of ground state and isomer is eventually established, internal transitions being now much faster than the time scales for β decay and neutron capture. Accordingly, the strength of the branching is only determined by the thermal conditions during the s process.

This behavior is particularly interesting with respect to current stellar models. In these models, the main s-process component, which accounts for the s abundances in the mass region $90 \leqslant A \leqslant 209$, is assumed to operate during helium shell burning in thermally pulsing stars on the asymptotic giant branch (AGB) of the Hertzsprung-Russell diagram [38]. In this scenario, neutron production and concordant s processing occur in two steps, by the $^{13}C(\alpha, n)^{16}O$ reaction during the hydrogen-burning stage at relatively low temperatures of $T \approx 1 \times 10^8$ K and during the subsequent helium burning by the $^{22}Ne(\alpha, n)^{25}Mg$ reaction at $T \approx 3 \times 10^8$ K.

From the above considerations it is obvious that [176]Lu is underproduced at the low temperatures of the first phase. This deficiency must, therefore, be compensated for during the helium-burning phase where the s process operates at higher temperatures. In this respect, the observed [176]Lu abundance can be used to constrain the temperature as well as the neutron exposure and the neutron density of this later episode.

VIII. SUMMARY

The neutron capture cross sections of [175]Lu and [176]Lu have been measured in the energy range of 3 to 225 keV with uncertainties of less than 1% (excluding the uncertainty of the [197]Au reference cross section). Conversion of these data into accurate Maxwellian averaged cross sections are important to a refined analysis of the s-process branching at $A = 176$, which is characterized by a fascinating interplay between nuclear and stellar nucleosynthesis aspects. Once the few remaining nuclear aspects are clarified, this branching will represent a crucial test for stellar models of the He shell burning phase in AGB stars.

ACKNOWLEDGMENTS

[1] F. Käppeler, G. Schatz, and K. Wisshak, Report KfK-3472, Kernforschungszentrum Karlsruhe, 1983 (unpublished).

[2] E. Anders and N. Grevesse, Geochim. Cosmochim. Acta **53**, 197 (1989).

[3] J. Best, H. Stoll, C. Arlandini, S. Jaag, F. Käppeler, K. Wisshak, A. Mengoni, G. Reffo, and T. Rauscher, Phys. Rev. C **64**, 015801 (2001).

[4] F. Käppeler, K. A. Toukan, M. Schumann, and A. Mengoni, Phys. Rev. C **53**, 1397 (1996).

[5] S. O'Brien, S. Dababneh, M. Heil, F. Käppeler, R. Plag, R. Reifarth, R. Gallino, and M. Pignatari, Phys. Rev. C **68**, 035801 (2003).

[6] H. Beer, F. Käppeler, K. Wisshak, and R. Ward, Astrophys. J. Suppl. Ser. **46**, 295 (1981).

[7] N. Klay, F. Käppeler, H. Beer, and G. Schatz, Phys. Rev. C **44**, 2839 (1991).

[8] C. Doll, H. G. Börner, S. Jaag, F. Käppeler, and W. Andrejtscheff, Phys. Rev. C **59**, 492 (1999).

[9] Z. Y. Bao, H. Beer, F. Käppeler, F. Voss, K. Wisshak, and T. Rauscher, At. Data Nucl. Data Tables **76**, 70 (2000).

[10] M. V. Bokhovko, V. N. Kononov, E. D. Poletaev, N. S. Rabotnov, and V. M. Timokhov, in *Nuclear Data for Science and Technology*, edited by S. Qaim (Springer, Berlin, 1992), p. 62.

[11] H. Beer, G. Walter, R. L. Macklin, and P. J. Patchett, Phys. Rev. C **30**, 464 (1984).

[12] V. S. Shorin, V. M. Gribunin, V. N. Kononov, and I. I. Sidorova, Astrophys. J. **7**, 286 (1973).

[13] R. L. Macklin and J. H. Gibbons, Phys. Rev. **159**, 1007 (1967).

[14] H. Beer and F. Käppeler, Phys. Rev. C **21**, 534 (1980).

[15] K. Wisshak, F. Voss, F. Käppeler, and L. Kazakov, Report FZKA-6961, Forschungszentrum Karlsruhe, 2004.

[16] K. Wisshak, K. Guber, F. Voss, F. Käppeler, and G. Reffo, Phys. Rev. C **48**, 1401 (1993).

[17] K. Wisshak, F. Voss, F. Käppeler, and G. Reffo, Phys. Rev. C **45**, 2470 (1992).

[18] K. Wisshak, K. Guber, F. Käppeler, J. Krisch, H. Müller, G. Rupp, and F. Voss, Nucl. Instrum. Methods A **292**, 595 (1990).

[19] JEFF-3.1 General Purpose Neutron File, May 2005, available at http://www.nea.fr/html/dbdata/JEFF/

[20] K. Wisshak, F. Voss, F. Käppeler, L. Kazakov, and M. Krtička, Report FZKA-6962, Forschungszentrum Karlsruhe, 2004 (unpublished).

[21] K. Wisshak, F. Voss, F. Käppeler, K. Guber, L. Kazakov, N. Kornilov, M. Uhl, and G. Reffo, Phys. Rev. C **52**, 2762 (1995).

[22] K. Wisshak, F. Voss, F. Käppeler, L. Kazakov, and G. Reffo, Report FZKA-5967, Forschungszentrum Karlsruhe, 1997 (unpublished).

[23] K. Wisshak, F. Voss, F. Käppeler, and G. Reffo, Phys. Rev. C **42**, 1731 (1990).

[24] F. Voss, K. Wisshak, C. Arlandini, F. Käppeler, L. Kazakov, and T. Rauscher, Phys. Rev. C **59**, 1154 (1999).

[25] F. H. Fröhner, Technical report, GA-8380, Gulf General Atomic, 1968 (unpublished).

[26] A. Gilbert and A. G. W. Cameron, Can. J. Phys. **43**, 1446 (1965).

[27] J. F. Mughabghab, M. Divadeenam, and N. E. Holden, in *Neutron Cross Sections* (Academic Press, New York, 1981), Vol. 1, Part A.

[28] F. Voss, K. Wisshak, K. Guber, F. Käppeler, and G. Reffo, Phys. Rev. C **50**, 2582 (1994).

[29] R. L. Macklin, private communication to S. F. Mughabghab, 1982; see also www.nndc.bnl.gov/nndc/ EXFOR 12720.002.

[30] W. Ratynski and F. Käppeler, Phys. Rev. C **37**, 595 (1988).

[31] K. Wisshak, F. Voss, F. Käppeler, L. Kazakov, and G. Reffo, Phys. Rev. C **57**, 391 (1998).

[32] J. Kopecky, J.-Ch. Sublet, J. A. Simpson, R. A. Forrest, and D. Nierop, Report INDC(NDS)-362, International Atomic Energy Agency, Vienna, 1997 (unpublished).

[33] H. Beer, F. Voss, and R. R. Winters, Astrophys. J. Suppl. Ser. **80**, 403 (1992).

[34] W. R. Zhao and F. Käppeler, Phys. Rev. C **44**, 506 (1991).

[35] N. Winckler, M. Heil, F. Käppeler, Phys. Rev. C (to be published).

[36] R. L. Macklin, D. Drake, and J. Malanify, Technical Report LA-7479-MS, Los Alamos National Laboratory, 1978 (unpublished).

[37] J. Lepine, R. Douglas, and H. Maia, Nucl. Phys. **A196**, 83 (1972).

[38] M. Busso, R. Gallino, and G. J. Wasserburg, Annu. Rev. Astron. Astrophys. **37**, 239 (1999).